Laminar Burning Velocity of the Dimethyl Carbonate–Air Mixture Formed by the Li-Ion Electrolyte Solvent

Henriksen, Mathias; Vågsæther, Knut; Gaathaug, Andre Vagner; Lundberg, Joachim; Forseth, Sissel; Bjerketvedt, Dag

University of South-Eastern Norway
Norwegian Defence Research Establishment

Henriksen, M., Vaagseather, K., Gaathaug, A. V., Lundberg, J., Forseth, S., & Bjerketvedt, D. (2020). *Laminar burning velocity of the dimethyl carbonate–air mixture formed by the Li-ion electrolyte solvent*. Combustion, Explosion, and Shock Waves, 56(4), pp. 383-393.
https://doi.org/10.1134/S0010508220040024

Publisher's version: DOI: 10.1134/S0010508220040024

ISSN 0010-5082, Combustion, Explosion, and Shock Waves, 2020, Vol. 56, No. 4, pp. 383–393. © Pleiades Publishing, Ltd., 2020.
Original Russian Text © M. Henriksen, K. Vaagseather, A.V. Gaathaug, J. Lundberg, S. Forseth, D. Bjerketvedt.

Laminar Burning Velocity of the Dimethyl Carbonate–Air Mixture Formed by the Li-Ion Electrolyte Solvent

M. Henriksen[a], K. Vaagseather[a], A. V. Gaathaug[a], J. Lundberg[a], S. Forseth[a], and D. Bjerketvedt[a]

UDC 536.46

Published in *Fizika Goreniya i Vzryva*, Vol. 56, No. 4, pp. 14–25, July–August, 2020.
Original article submitted December 23, 2019; revision submitted February 19, 2020; accepted for publication February 19, 2020.

Abstract: If a Li-ion cell fails and the electrolyte leaks out into air, a flammable premixed gas cloud can be formed. The electrolyte combustion energy is 65–70% of the total energy content of the cell. The main objective of this study is to determine the laminar burning velocity and the Markstein length for dimethyl carbonate and propane in a 20-liter explosion sphere with initial conditions at 100 kPa and 300 K. Five different stretch extrapolation models for the laminar burning velocity give practically the same result. The experimental results agree well with the previously published data and are slightly lower than the theoretical predictions. The laminar burning velocity for dimethyl carbonate is measured close to the saturation point under the initial conditions, which has not been previously reported.

Keywords: laminar burning velocity, dimethyl carbonate, Li-ion battery electrolyte, gas explosion.

DOI: 10.1134/S0010508220040024

INTRODUCTION

With the increasing need for clean and sustainable energy, Li-ion batteries (LIBs) have become a popular choice for energy storage. They are characterized by a high energy density and power compared to other rechargeable batteries. A challenge with the Li-ion technology is that it must have a protection circuit to ensure safety [1–3]. A combination of a flammable organic electrolyte with highly energetic materials present a potential for an accident [4]. In the last two decades, there have been several reports of fire- and explosion-related incidents caused by LIB failure [3–6].

The electrolyte is one of the main components in the Li-Ion cell/battery and consists of one or several organic carbonates (e.g., dimethyl carbonate) together with a Li-ion salt. Typical electrolytes are flammable. Mikolajczak et al. [7] estimated that the heat of combustion of the organic carbonates contributes 65–70% of the total energy content in the 18650 Li-ion cell, depending on the state of the charge.

In the Li-ion battery/cell, a thermal incident can be initiated by an internal or external short circuit, heat exposure, overload, over-discharge, overcharge, and mechanical abuse [7]. Such an incident can lead to the release of the electrolyte, hydrogen, carbon monoxide, methane, and other flammable species [6–12]. If these species mix with air, a flammable premixed gas cloud can be formed. If such a cloud is ignited, a gas explosion can occur.

Johnsplass [13] documented gas explosions in clouds of a vented electrolyte from the 18650 Li-ion cell that was externally heated to 425 K. The flame velocity observed on the high-speed video was up to 10 m/s. Figure 1 shows two still images from one of the exper-

[a] University of South-Eastern Norway, Porsgrunn, Telemark, Norway; mathias.henriksen@usn.no.
[b] Norwegian Defence Research Establishment, Oslo, Norway.

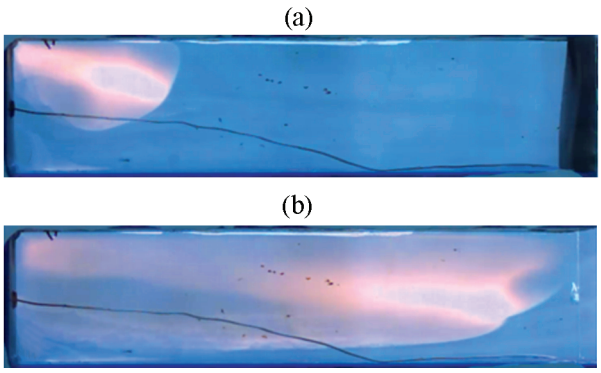

Fig. 1. Still images of an inhomogeneous flame propagating in a 0.45 × 0.10 × 0.10 m explosion channel; the 18650 Li-ion cell was externally heated until the combustible gas/mist vented; (a) image taken soon after ignition; (b) image taken when the flame reached the end of the channel.

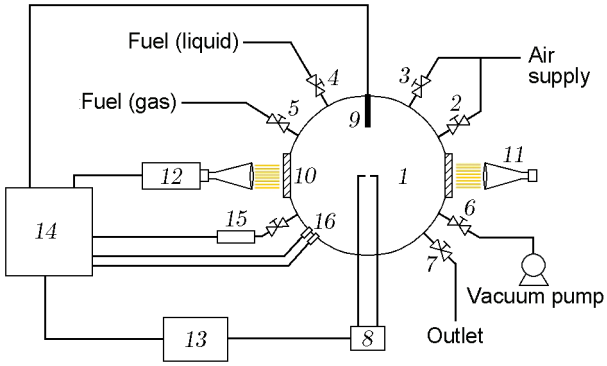

Fig. 2. Experimental setup: (*1*) explosion chamber; (*2*) oxidizer inlet; (*3*) flush inlet; (*4*) fuel (liquid) injection port; (*5*) fuel (gas) inlet; (*6*) vacuum port; (*7*) gas outlet; (*8*) ignition system; (*9*) thermocouple; (*10*) glass window (100 mm); (*11*) LED light source; (*12*) high-speed camera; (*13*) control/trigger unit; (*14*) data acquisition system; (*15*) ambient pressure transducer; (*16*) dual explosion pressure transducers.

iments. The cell lost roughly 2 g, which was assumed to be mostly the electrolyte. With an ambient temperature of 300 K and assuming a homogenous mixture in the channel, the concentration of dimethyl carbonate (DMC) in air would be approximately 8%. A closed volume combustion calculation shows that the explosion pressure can reach almost 1 MPa [14].

When studying flame propagation, the laminar burning velocity (LBV) is one of the essential parameters. At the beginning, the flame is usually slow and laminar with a flame speed in the order of 3–4 m/s. It propagates faster as the flame is affected by turbulence generated due to concentration differences, obstacles, self-generated turbulence, etc. [15]. The LBV is often a key parameter in modeling the turbulent flame speed and can be used to validate chemical kinetics [16–18]. Two previous studies on the LBV of DMC have been published. Bardin et al. [19] measured the LBV of DMC using a heat flux burner at different conditions. Persis et al. [20] measured the LBV of DMC in an explosion sphere with the initial conditions at 318 K and 1 atm.

In this study, a typical 20-liter explosion sphere is used to determine the laminar burning velocity and Markstein length for DMC and propane. The experiments are performed in a typical manner, as described in other studies [21–26]. The experimental results are compared with previously published studies and with theoretical calculations. The initial conditions for all experiments were the absolute pressure of 100 kPa and temperature of 300 K. This paper is an extended version of the work presented at the 9th International Seminar on Fire and Explosion Hazards in April 2019 [27].

MATERIALS AND METHODS

The experimental setup (20-liter explosion sphere) is schematically shown in Fig. 2. A detailed description of the setup and the procedure has been previously published [27]. A heating jacket controls the ambient temperature in the sphere. In the bottom of the sphere, there is a heated plate for evaporating liquids. Two identical pressure transducers measure the explosion pressure, and a separate pressure transducer records the ambient pressure during sphere evacuation and filling. Dedicated inlets are used for the oxidizer, liquid fuel, and gaseous fuel to reduce uncertainties in the fuel–air concentration. DMC has a purity above 99% and propane has a purity above 99.95%. An ignition coil generates a spark between two metal wires with a variable gap.

A focused shadowgraphy technique [28] was used to enhance the visibility of the propagating flame, which was recorded with a high-speed camera operating at 20 000 fps. Image processing and data analysis were undertaken using the tool/code generated in Python.

Image background subtraction was used to remove noise that could potentially influence flame front detection. As the shadowgraphy technique was used, the images contain two intensity gradients corresponding to the inner and outer perimeter of the flame. The outer perimeter was chosen because it is closer to the unburnt mixture. In each image, the threshold that separates the flame from the background is set individually. The perimeter of the flame is then fitted to a circle using the least square minimization to obtain the overall radius.

Dette er en postprint-versjon/This is a postprint version.
DOI til publisert versjon/DOI to published version: 10.1134/S0010508220040024

Table 1. Stretch extrapolation models

Model name/description	Expression	Reference
Linear stretch model (LS)	$S_b = S_b^0 - L_b\kappa$	[30, 31]
Linear curvature model (LC)	$S_b = S_b^0\left(1 - \frac{2L_b}{r_f}\right)$	[32, 33]
Nonlinear model with three fitting parameters (N3P)	$S_b = S_b^0\left(1 - \frac{2L_b}{r_f} + \frac{c}{r_f^2}\right)$	[29]
Nonlinear model in the expansion form (NQ)	$S_b^0 + c = r_f + 2L_b\ln(r_f) - \frac{4L_b^2}{r_f} - \frac{8L}{3r}$	[34]
Quasi-steady nonlinear model (NE)	$\left(\frac{S_b}{S_b^0}\right)^2 \ln\left(\frac{S_b}{S_b^0}\right) = -\frac{2L_b\kappa}{S_b^0}$	[35, 36]

Table 2. Implicit functions of the flame radius derived from the expressions in Table 1

Model name	Implicit dependence $r_f(t)$
LS	$r_f = S_b^0 t - 2L_b\ln r_f + C_{\mathrm{st}}$
LC	$r_f - S_b^0 t - 2L_b\ln(r_f - 2L_b) + C_{\mathrm{st}}$
N3P ($A > 0$)	$r_f = S_b^0 t - L_b(r_f^2 - 2L_b r_f + c) - \frac{2L_b^2 - c}{2\sqrt{A}}\ln\left(-\frac{r_f + \sqrt{A} + L_b}{r_f + \sqrt{A} - L_b}\right) + C_{\mathrm{st}}$
N3P ($A < 0$)	$r_f = S_b^0 t - L_b(r_f^2 - 2L_b r_f + c) - \frac{2A}{\sqrt{-A}}\arctan\left(\frac{r - L_b}{\sqrt{-A}}\right) + C_{\mathrm{st}}$
	$A - L_b^2 - c$
NQ	$r_f = S_b^0 t + c - 2L_b\ln(r_f) + \frac{4L_b^2}{r_f} + \frac{8L_b^3}{3r_f^2}$

The code saves the set of the images together with the temporal evolution of the radius.

The first step in the post-processing tool/code is to set the radius range to be considered in the calculations. The lowest radius is set to 10 mm but may be changed to fit the product of the Markstein number Ma and Karlovitz number Ka ($\mathrm{Ma}\cdot\mathrm{Ka}$) in the interval from -0.05 to 0.15 [29]. The radius above 37.5 mm is removed due to an increase in the variation in the data. From the conditioned radii, the laminar flame speed and the Markstein length are calculated. Table 1 shows the stretch extrapolation models used in this study.

By representing the flame speed S_b as the derivative $\frac{dr_f}{dt}$, the expressions in Table 1 can be written as differential equations. In particular, the equation below shows the differential equation for the linear stretch model:

$$\frac{dr_f}{dt}\left(1 + \frac{2L_b}{r_f}\right) = S_b^0.$$

Dette er en postprint-versjon/This is a postprint version.
DOI til publisert versjon/DOI to published version: 10.1134/S0010508220040024

Here r_f [m] is the flame radius, t [s] is the time, and L_b [m] is the Markstein length for the burnt gas. The solution to the differential equation above yields an implicit function of the flame radius. This function can be fitted to the measured variation of the radius in time with the least square minimization method. Chen [16] and Liu et al. [26] previously published a similar method for the LS model. Table 2 shows the implicit functions for the expressions in Table 1, except for the NE model.

The NQ model in the expansion form (see Table 1) is already expressed as an implicit function of the flame radius. An analytical solution to the differential equation of the NE model could not be found. Liu et al. [36] proposed a method for solving the NE model, but the regression is on the flame speed and stretch rate relation. This method is represented by the equations

$$\kappa = AS_b - BS_b^2 \ln(S_b^2),$$

$$A = \ln(S_b^0)/L_b S_b^0, \quad B = (1/2)L_b S_b^0,$$

$$S_b^0 = \exp(A/2B), \quad L_b = (1/2)BS_b^0,$$

where κ [s^{-1}] is the stretch rate and A [m^2] is the area. To reduce noise from the image processing, the flame radius and flame speed were post-filtered with the Savitzky–Golay smoothing algorithm [37] and used in the NE method by Liu et al. [36]. All other models were fitted using the raw data from the image processing.

The equilibrium states and the LBV for constant-pressure combustion were calculated in the chemical kinetics, thermodynamics, and transport process simulation tool Cantera (version 2.3.0) [38]. For a one-dimensional freely propagating planar flame, the Cantera routine called FreeFlame was used to calculate the LBV. Two different reaction mechanisms for DMC oxidation were used for comparison: those of Glaude et al. [39] and Sun et al. [40]. A constant-pressure equilibrium solver was used to determine the density ratio for DMC and propane. The reaction mechanism of Glaude et al. [39] and the GRI-Mech 3.0 mechanism [41] were used in the equilibrium calculations.

RESULTS

Tables 3 and 4 summarize the results for propane and DMC, respectively. Propane has the highest measured LBV and flame speed at the equivalence ratio $\phi = 1.2$ of the four different concentrations. Comparing the DMC results, the highest LBV and flame speed were obtained at $\phi = 1.04$. The LBV of DMC is nearly constant in the concentration range $1.0 \leqslant \phi \leqslant 1.2$. For both fuels, the highest LBV values are located near stoichiometric concentrations, with the highest values slightly on the rich side, which could be expected.

For propane, there is only a small difference in the laminar flame speed between different models. By comparing the average value for each concentration, the variation is between ± 41 mm/s for $\phi = 0.82$ and ± 18 mm/s for $\phi = 1.2$. For DMC, the variation is somewhat larger, from ± 90 mm/s for $\phi = 0.84$ to ± 2.4 mm/s for $\phi = 1.43$. For the relatively high variation at $\phi = 0.84$ for DMC, the $\mathrm{Ma} \cdot \mathrm{Ka}$ value is equal to 0.24, which is above the recommended value of 0.15. It was not possible to reduce the $\mathrm{Ma} \cdot \mathrm{Ka}$ value by simply removing the smaller radii. The result from the experiment was still kept because the variation in the LBV between the models was not significant (see Table 4).

There is a larger variation in the Markstein length between all models compared to the variation in the laminar burning velocity. By comparing the average L_b value for each concentration, the variation for propane is between ± 0.4 mm for $\phi = 0.82$ and ± 0.1 mm for $\phi = 1.2$. DMC had a higher variation compared to propane: from ± 1.0 mm for $\phi = 0.84$ to ± 0.02 mm for $\phi = 1.43$. The maximum and minimum variations of the Markstein length corresponds to the same experiments with the maximum and minimum variations in the laminar flame speed.

The coefficient of determination R^2 is almost identical for the four stretch models used to fit the dependence of the flame radius on time. At the same time, the NE method proposed by Liu et al. [26] yields smaller R^2 values in all experiments. As the models are fitted based on different parameters, it is difficult to compare the R^2 values between the NE method and the other four models.

DISCUSSION

When using an explosion sphere to determine the flame speed, the thermal diffusion, hydrodynamic instabilities, and buoyancy can cause instabilities and may influence the flame propagation [21, 42]. Choosing the concentration close to stoichiometry ($\phi = 1.0$) will reduce instabilities. For some of the rich mixtures, small flame front instabilities can be seen in Fig. 3. These instabilities may cause small errors in the calculated LBV. Regarding the buoyancy effects, Ronney and Wachman [43] reported that buoyancy would not cause any significant errors in the radius measurements in the experiments with LBV values above 150 mm/s. As the measured LBV is above 200 mm/s in all experiments of the present study, the discrepancies due to buoyancy are considered as negligible.

Table 3. Summary of results for propane–air mixture burning at the initial temperature of 300 K and initial absolute pressure of 100 kPa

ϕ	Flame parameters	Stretch extrapolation model				
		LS	LC	N3P	NE	NQ
0.82	S_b^0, mm/s	2047.2	2000.4	2004.3	2004.5	1977.0
	L_b, mm	1.80	1.31	1.35	1.34	1.11
	S_u^0, mm/s	287.0	280.5	281.0	281.1	277.2
	R^2	0.999997	0.999998	0.999998	0.999998	0.995362
0.99	S_b^0, mm/s	2976.4	2932.3	2974.2	2 935.5	2905.7
	L_b, mm	1.39	1.08	1.38	1.10	0.94
	S_u^0, mm/s	378.8	373.1	378.5	373.6	369.8
	R^2	0.999999	0.999999	0.999999	0.999999	0.991300
1.20	S_b^0, mm/s	3139.5	3120.9	3138.5	3121.8	3108.0
	L_b, mm	0.84	0.72	0.84	0.72	0.65
	S_u^0, mm/s	396.0	393.7	395.9	393.8	392.1
	R^2	0.999999	0.999999	0.999999	0.999999	0.978764
1.43	S_b^0, mm/s	1926.5	1925.6	1924.2	1925.6	1896.2
	L_b, mm	−0.22	−0.23	−0.24	−0.23	−0.39
	S_u^0, mm/s	252.0	251.9	251.7	251.9	248.1
	R^2	0.999998	0.999998	0.999998	0.999998	0.563832

Pressure changes can also cause hydrodynamic instabilities. However, in the recorded pressure within the radius measurement range, no significant pressure increase was detected. Ignition-induced instabilities often propagate along with the flame development [44]. For this reason, the experiments with non-spherical flame propagation were rejected. By varying the spark gap in the interval 0.5–2.0 mm for different concentrations, the ignition-induced instabilities were reduced. Figure 3 shows that the flame exhibits spherical propagation in most experiments and has a smooth surface with relatively few wrinkles.

Figure 4a shows the unfiltered measured radii and the regression curves, except for the NE model. The light tone markers are all measured radii, and the black markers are the radii used in the regression study. The radii below 10 mm were automatically removed because of the relatively large change in the flame speed (Fig. 4b). Kelley et al. [44] reported a similar observation when investigating the critical radius necessary to sustain flame propagation. The flame propagates initially with a high velocity due to ignition, but decelerates as it propagates. At a certain flame radius, the flame speed starts to increase until it reaches a flame speed that approaches the LBV. For radii above 10 mm, the flame radius increased almost linearly in time for most of the experiments; therefore, this value was chosen as the initial minimum radius. More experimental points were removed for which the product of the Markstein number and the Karlovitz number was outside the recommended range of −0.05 to 0.15 proposed by Wu et al. [29], who demonstrated that the LBV measurement should be conducted within the mentioned range to minimize the extrapolation uncertainties:

$$\mathrm{Ma}_{\mathrm{linear}}\mathrm{Ka}_{\mathrm{mid}} = \frac{L_b}{\delta_L}\frac{\kappa\delta_L}{S_b} = \frac{2L_{b,\mathrm{linear}}}{r_{f,\mathrm{mid}}}$$

(δ_L is the laminar flame thickness). In Fig. 4a, all models fit equally well with the measured radii, which is expected based on the R^2 value in Tables 3 and 4. Based on the results in Tables 3 and 4, the models for extrapolating the laminar flame speed and burning velocity yield fairly similar results, which are almost independent of the model if used within the interval $-0.05 < \mathrm{Ma}\cdot\mathrm{Ka} < 0.15$.

Figure 5a shows the propane–air combustion results compared with previously published studies [22–26, 45]. The DMC results are also compared in Fig. 5b to the results of [19] and with the predictions by two reaction mechanisms [39, 40]. For comparison of the experimental results, only the LS model was used because it was this model that was used in the previous studies. It is worth mentioning that the variation in the LBV between the methods is significantly smaller (±5 mm/s at most) than the variation between the different studies (±30 mm/s on the average).

Dette er en postprint-versjon/This is a postprint version.
DOI til publisert versjon/DOI to published version: 10.1134/S0010508220040024

Table 4. Summary of results for DMC–air mixture burning at the initial temperature of 300 K and initial absolute pressure of 100 kPa

ϕ	Flame parameters	Stretch extrapolation model				
		LS	LC	N3P	NE	NQ
0.84	S_b^0, mm/s	1895.1	1804.6	1729.3	1814.8	1783.9
	L_b, mm	2.84	1.79	0.97	1.86	1.53
	S_u^0, mm/s	250.8	238.8	228.9	240.2	236.1
	R^2	0.999968	0.999987	0.999993	0.999984	0.991726
1.01	S_b^0, mm/s	2436.2	2383.8	2395.3	2388.3	2361.5
	L_b, mm	1.74	1.28	1.38	1.30	1.11
	S_u^0, mm/s	293.6	287.3	288.6	287.8	284.6
	R^2	0.999997	0.999998	0.999998	0.999998	0.994419
1.04	S_b^0, mm/s	2491.8	2446.3	2464.8	2450.0	2425.3
	L_b, mm	1.57	1.18	1.34	1.21	1.03
	S_u^0, mm/s	300.3	294.8	297.0	295.2	292.2
	R^2	0.999998	0.999998	0.999998	0.999998	0.993317
1.13	S_b^0, mm/s	2494.2	2474.8	2491.8	2475.9	2461.6
	L_b, mm	0.98	0.81	0.96	0.82	0.73
	S_u^0, mm/s	297.3	294.9	297.0	295.1	293.4
	R^2	0.999998	0.999998	0.999998	0.999998	0.988313
1.16	S_b^0, mm/s	2522.3	2497.8	2529.2	2499.4	2482.3
	L_b, mm	1.10	0.90	1.14	0.90	0.80
	S_u^0, mm/s	300.9	298.0	301.8	298.2	296.2
	R^2	0.999996	0.999996	0.999996	0.999996	0.962149
1.32	S_b^0, mm/s	2144.8	2141.5	2143.8	2141.6	2140.3
	L_b, mm	0.41	0.38	0.40	0.38	0.37
	S_u^0, mm/s	261.0	260.6	260.9	260.7	260.5
	R^2	0.999999	0.999999	0.999999	0.999999	0.910555

The propane results are compared well with the previously published data, which indicates that the experimental setup and method provide acceptable results. The experimental results for DMC in this study match reasonably well with the data reported in [19]. Although there are only a few overlapping points in Fig. 5, the trend from the two datasets shares the same curve profile.

The results of this study include LBV values at 300 ± 2 K with the equivalence ratios $\phi > 1$, which have not been reported previously. For the LBV at $\phi = 1.32$, the partial pressure in that experiment (8.5 kPa at 302 K) was close to the estimated DMC vapor pressure of 8.8 kPa in [46]. The small pressure difference may cause some uncertainties of the concentration in the experiment.

The reaction mechanism of Sun et al. [40] agrees with the experimental results better than that by Glaude et al. [39]. Both calculations predict a higher LBV value than the results for DMC from both experimental studies. It is uncertain what is the reason for this discrepancy. Meanwhile, the radiative heat loss can contribute to the discrepancy between simulations and experiments, according to Chen [16].

Figure 6 shows comparisons of the explosion pressure (a) and the rate of explosion pressure rise (b) for propane and DMC. DMC has the highest explosion pressure of 0.94 MPa, which is higher than that of propane. However, propane has the higher rate of explosion pressure rise of 43 MPa/s. The higher rate of explosion pressure rise for propane is consistent with the LBV value. In Fig. 6, there are more data points than in Fig. 5 because Fig. 6 also shows the LBV measurements earlier rejected due to pronounced non-sphericity of flame propagation.

In the case of a leak of DMC into a confined space, the vapor concentration is determined by the vapor–liquid equilibrium, if the leaked amount is sufficient.

Dette er en postprint-versjon/This is a postprint version.
DOI til publisert versjon/DOI to published version: 10.1134/S0010508220040024

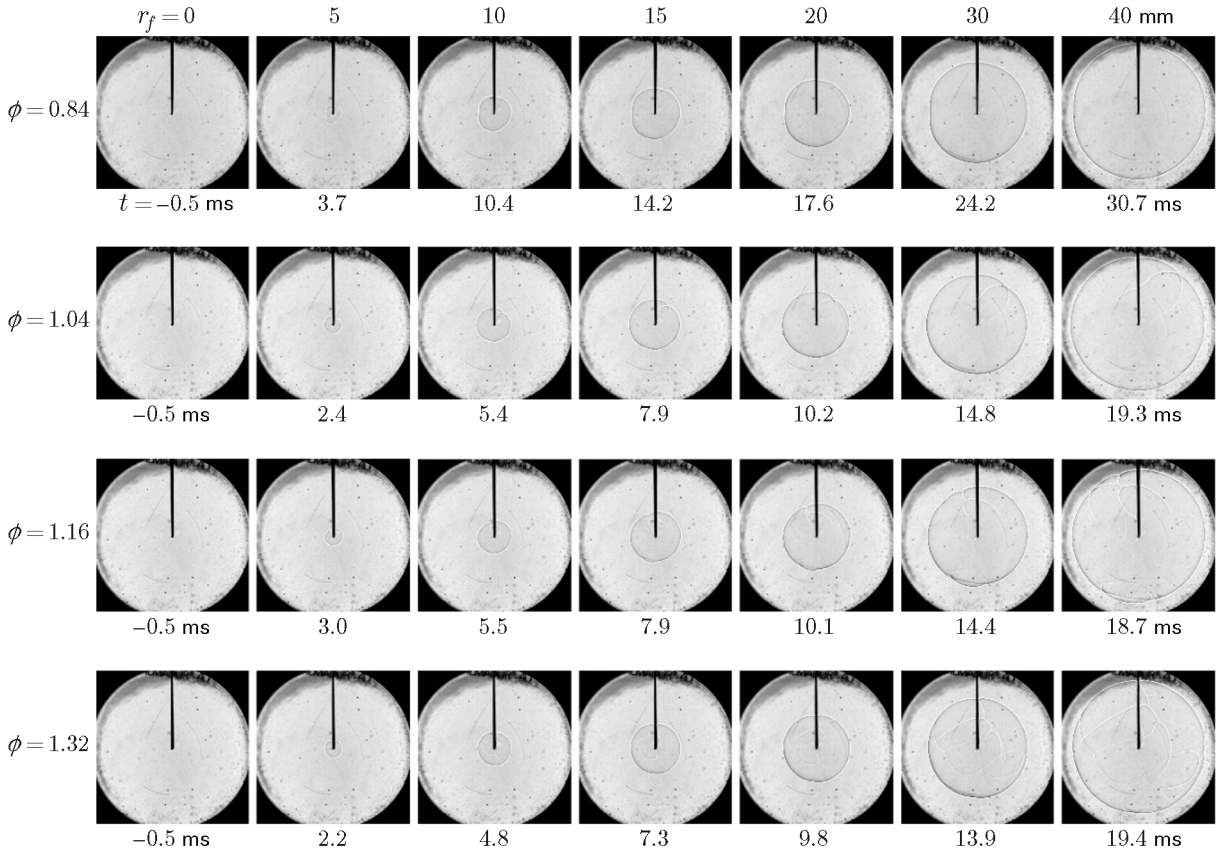

Fig. 3. Shadowgraph images of DMC combustion: the initial conditions are the temperature of 300 K and absolute pressure of 100 kPa.

At 1 atm and 300 K, the equilibrium vapor pressure for DMC corresponds to $\phi = 1.25$, which is above the stoichiometric value. At the same time, it means that the fuel–air mixture will never exceed the upper explosion limit under these conditions. An extra amount of DMC above the vapor–liquid equilibrium concentration induces vapor condensation, and the concentration of DMC in the gas phase is practically the same. The partial density of the DMC vapor at $\phi = 1.25$ under the above-mentioned conditions is 0.29 g/liter. The equilibrium explosion pressure at this concentration is 0.93 MPa, which is very close to the maximum explosion pressure recorded in this study. Also note that the ignition energy at $\phi = 1.25$ is close to its minimum value.

CONCLUSIONS

The laminar flame speed, Markstein length, and laminar burning velocity for propane and dimethyl carbonate at different concentrations were determined in a 20-liter explosion sphere at the initial temperature of 300 K and the initial absolute pressure of 100 kPa. If the product of the Markstein and Karlovitz numbers is within −0.05–0.15 for each experiment, then the results for the laminar flame speed are practically independent on the stretch extrapolation model used. The measured laminar burning velocities agree with the previously published data. The measurement procedure and the experimental setup provide consistent results and offer a suitable method for determining the laminar burning velocities.

For dimethyl carbonate, the highest laminar burning velocity of 300 mm/s was found at the fuel–air equivalence ratio of 1.04. This is slightly on the rich side, as expected. In this study of the laminar burning velocity, the concentration range for DMC is wider than that studied by Bardin et al. [19]. The laminar burning velocity measured near the saturated vapor pressure at 302 K is 261 mm/s.

The reaction mechanism of Sun et al. [40] yielded the laminar burning velocity closer to the experimental results than that of Glaude et al. [39]. Both reaction mechanisms overpredicted the laminar burning veloc-

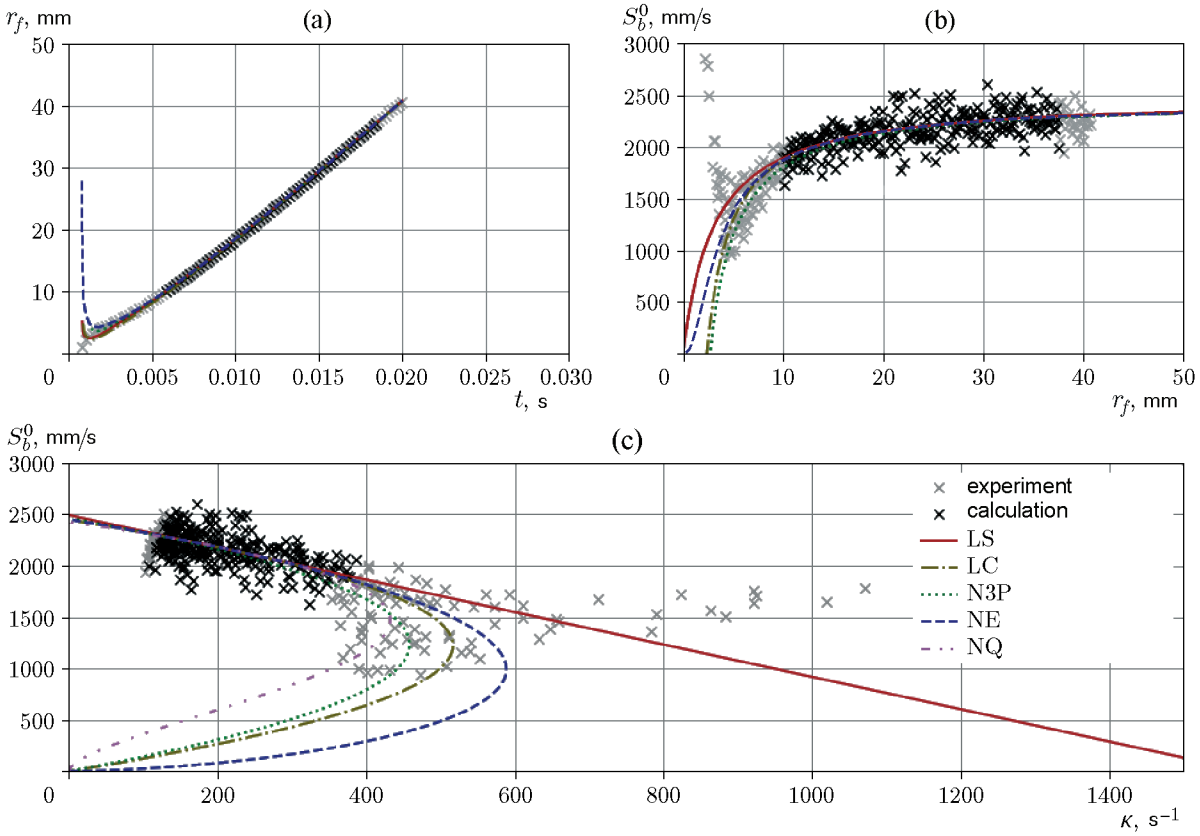

Fig. 4. Comparison of models used for extrapolation of LBV values: DMC, $\phi = 1.04$, the initial conditions are the temperature of 300 K and absolute pressure of 100 kPa.

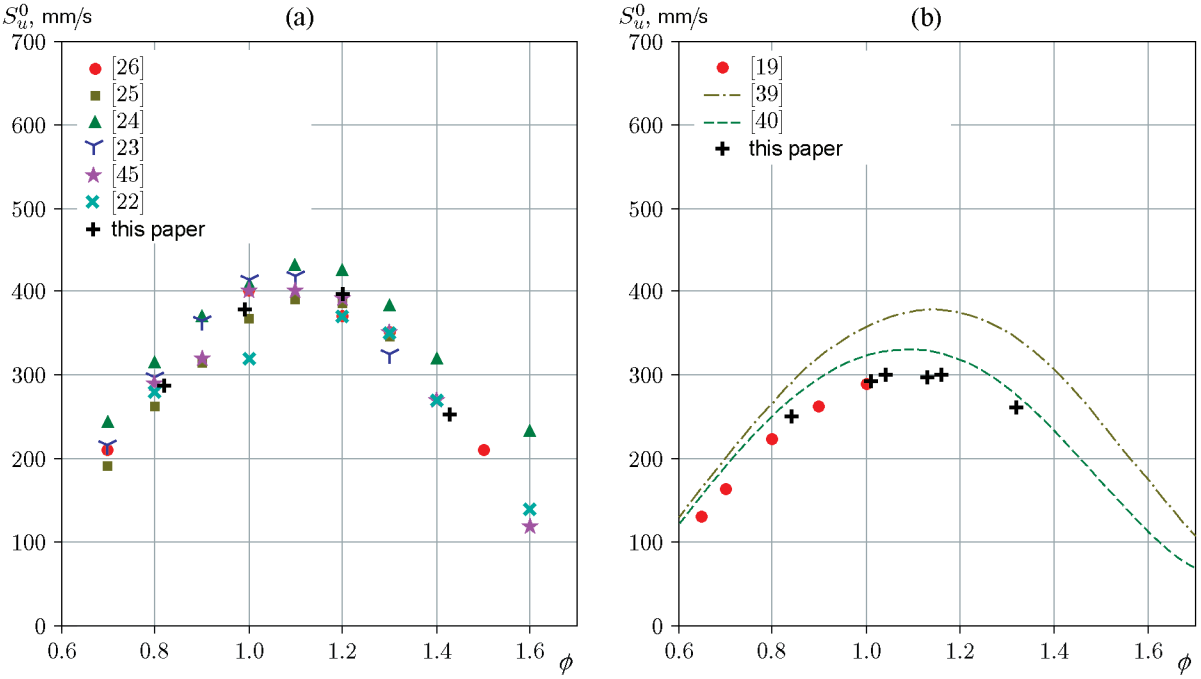

Fig. 5. Measured laminar burning velocity versus the equivalence ratio: (a) propane flame (comparison with previously reported results); (b) DMC flame (comparison with previously reported results and predictions with two reaction mechanisms); the initial conditions are the temperature of 300 K and absolute pressure of 100 kPa.

Dette er en postprint-versjon/This is a postprint version.
DOI til publisert versjon/DOI to published version: 10.1134/S0010508220040024

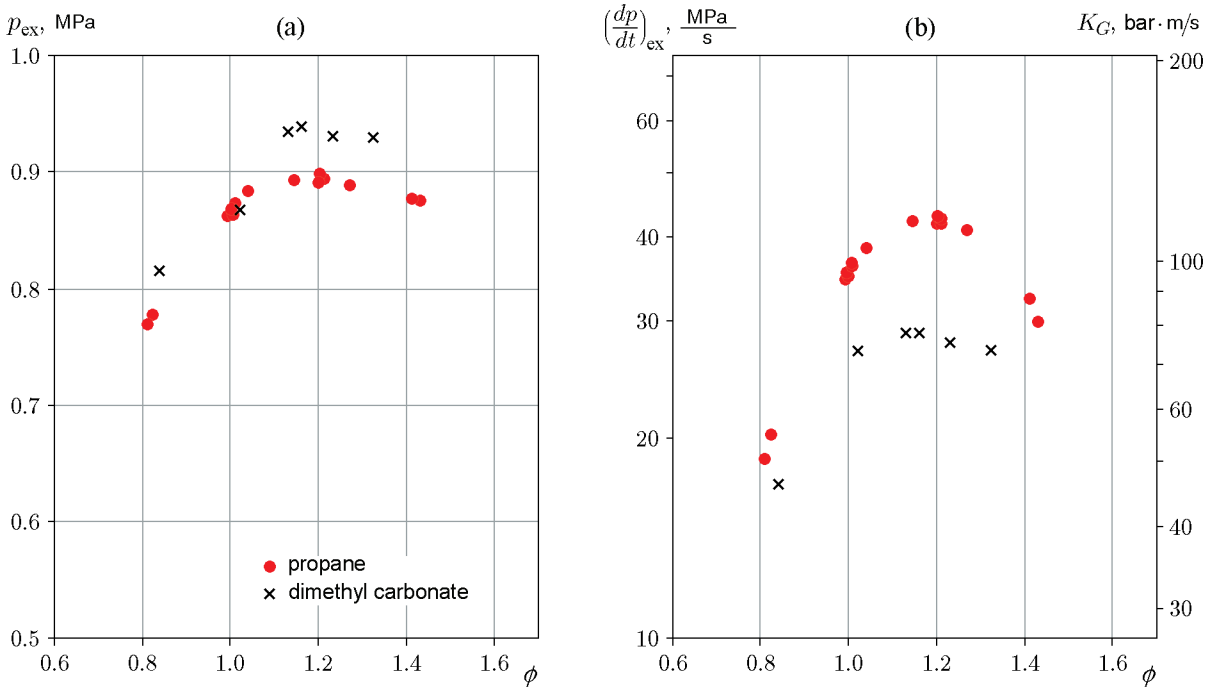

Fig. 6. Comparison of the explosion characteristics for propane and DMC: (a) explosion pressure; (b) rate of explosion pressure rise; K_G is the deflagration index; the initial conditions are the temperature of 300 K and absolute pressure of 100 kPa.

ities compared to the experimental results. This disagreement may be due to the radiative heat losses in the explosion sphere compared to the adiabatic conditions assumed in the theoretical calculation.

Dimethyl carbonate has the higher maximum explosion pressure of 0.94 MPa, and propane exhibits the higher rate of explosion pressure rise (43 MPa/s), which is consistent with the higher burning velocities in propane–air mixtures.

This work was performed at MoZEES, a Norwegian Centre for Environment-friendly Energy Research (FME), co-sponsored by the Research Council of Norway (project number 257653) and 40 partners from research, industry, and public sector.

Special thanks to Nabiha Chaumeix from CNRS-INSIS Laboratory ICARE for demonstrating the ICAREs experimental method and software for determining the laminar burning velocity. The development of the image and post-processing code was inspired by the helpful discussion with Nabiha Chaumeix.

REFERENCES

1. N.-S. Choi, Z. Chen, S. A. Freunberger, et al., "Challenges Facing Lithium Batteries and Electrical Double-Layer Capacitors," Angew. Chem. Int. Ed. **51**, 9994–10024 (2012); DOI: 10.1002/anie.201201429.
2. What's the Best Battery? (Battery Univ., 2017); http://batteryuniversity.com/learn/archive/whats_the_best_battery.
3. D. Lisbona and T. Snee, "A Review of Hazards Associated with Primary Lithium and Lithium-Ion Batteries," Process Saf. Environ. Prot. **89** (6), 434–442 (2011); DOI: 10.1016/j.psep.2011.06.022.
4. P. G. Balakrishnan, R. Ramesh, and T. Prem Kumar, "Safety Mechanisms in Lithium-Ion Batteries," J. Power Sources **155** (2), 401–414 (2006); DOI: 10.1016/j.jpowsour.2005.12.002.
5. S. Abada, G. Marlair, A. Lecocq, et al., "Safety Focused Modeling of Lithium-Ion Batteries: A Review," J. Power Sources **306**, 178–192 (2016); DOI: 10.1016/j.jpowsour.2015.11.100.
6. Q. Wang, P. Ping, X. Zhao, et al., "Thermal Runaway Caused Fire and Explosion of Lithium Ion Battery," J. Power Sources **208**, 210–224 (2012); DOI: 10.1016/j.jpowsour.2012.02.038.
7. C. Mikolajczak, M. Kahn, K. White, and R. T. Long, *Lithium-Ion Batteries Hazard and Use Assessment*, (Springer, Boston, 2011); DOI: 10.1007/978-1-4614-3486-3.
8. S. J. Harris, A. Timmons, and W. J. Pitz, "A Combustion Chemistry Analysis of Carbonate Solvents Used in Li-Ion Batteries," J. Power Sources **193** (2), 855–858 (2009); DOI: 10.1016/j.jpowsour.2009.04.030.

9. C. C. Crafts, D. H. Doughty, J. McBreen, and E. P. Roth, "Advanced Technology Development Program for Lithium-Ion Batteries: Thermal Abuse Performance of 18650 Li-Ion Cells," Sandia Report No. 2004-1584 (Sandia Nat. Lab., 2004); DOI: 10.2172/918751.
10. P. Ribière, S. Grugeon, M. Morcrette, et al., "Investigation on the Fire-Induced Hazards of Li-Ion Battery Cells by Fire Calorimetry," Energy Envir. Sci. **5**, 5271–5280 (2012); DOI: 10.1039/C1EE02218K.
11. A. W. Golubkov, S. Scheikl, R. Planteu, et al., "Thermal Runaway of Commercial 18650 Li-Ion Batteries with LFP and NCA Cathodes—Impact of State of Charge and Overcharge," RSC Advances **5**, 57171–57186 (2015); DOI: 10.1039/C5RA05897J.
12. F. Colella et al., "Analysis of Combustion Hazards due to Catastrophic Failures in Lithium-Ion Battery Packs," in *Proc. of the 7th Int. Seminar Fire and Explosion Hazards* (Research Publ. Services, 2013), pp. 575–584; DOI: 10.3850/978-981-07-5936-0_09-02.
13. J. Johnsplass, *Lithium-Ion Battery Safety* (Univ. of South-Eastern Norway, 2017).
14. M. Henriksen, K. Vaagsaether, J. Lundberg, et al., "Explosion Characteristics for Li-Ion Battery Electrolytes at Elevated Temperatures," J. Hazard. Mater. **371**, 1–7 (2019); DOI: 10.1016/j.jhazmat.2019.02.108.
15. D. Bjerketvedt, J. R. Bakke, and K. Van Wingerden, "Gas Explosion Handbook," J. Hazard. Mater. **52** (1), 1–150 (1997).
16. Z. Chen, "On the Accuracy of Laminar Flame Speeds Measured from Outwardly Propagating Spherical Flames: Methane/Air at Normal Temperature and Pressure," Combust. Flame **162** (6), 2442–2453 (2015); DOI: 10.1016/j.combustflame.2015.02.012.
17. J. Huo, S. Yang, Z. Ren, et al., "Uncertainty Reduction in Laminar Flame Speed Extrapolation for Expanding Spherical Flames," Combust. Flame **189**, 155–162 (2018); DOI: 10.1016/j.combustflame.2017.10.032.
18. Ö. L. Gülder, "Correlations of Laminar Combustion Data for Alternative S. I. Engine Fuels," SAE Tech. Paper No. 841000, (1984); DOI: 10.4271/841000.
19. M. E. Bardin et al., "Laminar Burning Velocities of Dimethyl Carbonate with Air," Energy Fuels **27** (9), 5513–5517 (2013); DOI: 10.1021/ef401108a.
20. S. De Persis, N. Chaumeix, Y. Fernandes, et al., "Experimental and Theoretical Determination of DMC/Air Flame Velocities," in *11th Int. Conf. on Chemical Kinetics, Orleans, 2019*, Poster No. 30.
21. A. A. Konnov, A. Mohammad, V. R. Kishore, et al., "A Comprehensive Review of Measurements and Data Analysis of Laminar Burning Velocities for Various Fuel + Air Mixtures," Prog. Energy Combust. Sci. **68**, 197–267 (2018); DOI: 10.1016/j.pecs.2018.05.003.
22. L.-K. Tseng, M. A. Ismail, and G. M. Faeth, "Laminar Burning Velocities and Markstein Numbers of Hydrocarbon–Air Flames," Combust. Flame **95** (4), 410–426 (1993); DOI: 10.1016/0010-2180(93)90007-P.
23. G. Jomaas, X. L. Zheng, D. L. Zhu, and C. K. Law, "Experimental Determination of Counterflow Ignition Temperatures and Laminar Flame Speeds of C_2–C_3 Hydrocarbons at Atmospheric and Elevated Pressures," Proc. Combust. Inst. **30** (1), 193–200 (2005); DOI: 10.1016/j.proci.2004.08.228.
24. C. Tang, J. Zheng, Z. Huang, and J. Wang, "Study on Nitrogen Diluted Propane–Air Premixed Flames at Elevated Pressures and Temperatures," Energy Convers. Manage **51**, 288–295 (2010); DOI: 10.1016/j.enconman.2009.09.024.
25. W. Lowry, J. de Vries, M. Krejci, et al., "Laminar Flame Speed Measurements and Modeling of Pure Alkanes and Alkane Blends at Elevated Pressures," J. Eng. Gas Turbines Power **133** (9), ID 091501 (2011); DOI: 10.1115/1.4002809.
26. Q. Liu, Y. Zhang, F. Niu, and L. Li, "Study on the Flame Propagation and Gas Explosion in Propane/Air Mixtures," Fuel **140**, 677–684 (2015); DOI: 10.1016/j.fuel.2014.09.123.
27. M. Henriksen, K. Vaagsaether, A. V. Gaathaug, et al., "Laminar Burning Velocity Measurements for an Outwardly Propagating Flame of Dimethyl Carbonate and Air Mixtures," in *Proc. of the 9th Int. Seminar on Fire and Explosion Hazards, St Petersburg, Russia, 2019* (Peter the Great St. Petersburg Polytech. Univ. Press, 2019), Vol. 1, pp. 161–172; DOI: 10.18720/spbpu/2/k19-29.
28. G. S. Settles, *Schlieren and Shadowgraph Techniques: Visualizing Phenomena in Transparent Media* (Springer, Berlin–New York, 2001).
29. F. Wu, W. Liang, Z. Chen, et al., "Uncertainty in Stretch Extrapolation of Laminar Flame Speed from Expanding Spherical Flames," Proc. Combust. Inst. **35**, 663–670 (2015); DOI: 10.1016/j.proci.2014.05.065.
30. C. K. Law, *Combustion Physics* (Cambridge Univ. Press, 2006).
31. F. A. Williams, *Combustion Theory* (Chapman and Hall/CRC, Boulder, 2018).
32. G. H. Markstein, *Nonsteady Flame Propagation* (Elsevier Sci., Burlington, 2014).
33. Z. Chen, "On the Extraction of Laminar Flame Speed and Markstein Length from Outwardly Propagating Spherical Flames," Combust. Flame **158**, 291–300 (2011); DOI: 10.1016/j.combustflame.2010.09.001.
34. A. P. Kelley, J. K. Bechtold, and C. K. Law, "Premixed Flame Propagation in a Confining Vessel with Weak Pressure Rise," J. Fluid Mech. **691**, 26–51 (2012); DOI: 10.1017/jfm.2011.439.
35. A. P. Kelley and C. K. Law, "Nonlinear Effects in the Extraction of Laminar Flame Speeds from Expanding Spherical Flames," Combust. Flame **156**, 1844–1851 (2009); DOI: 10.1016/j.combustflame.2009.04.004.

36. Q. Liu, X. Chen, Y. Shen, and Y. Zhang, "Parameter Extraction from Spherically Expanding Flames Propagated in Hydrogen/Air Mixtures," Int. J. Hydrogen Energy **44** (2), 1227–1238 (2019); DOI: 10.1016/j.ijhydene.2018.11.004.
37. A. Savitzky and M. J. E. Golay, "Smoothing and Differentiation of Data by Simplified Least Squares Procedures," Anal. Chem. **36** (8), 1627–1639 (1964); DOI: 10.1021/ac60214a047.
38. D. G. Goodwin, H. K. Moffat, and R. L. Speth, "Cantera: An Object-Oriented Software Toolkit for Chemical Kinetics, Thermodynamics, and Transport Processes. Version 2.3.0," (2017); DOI: 10.5281/zenodo.170284.
39. P. A. Glaude, W. J. Pitz, and M. J. Thomson, "Chemical Kinetic Modeling of Dimethyl Carbonate in an Opposed-Flow Diffusion Flame," Proc. Combust. Inst. **30** (1), 1111–1118 (2005); DOI: 10.1016/j.proci.2004.08.096.
40. W. Sun, B. Yang, N. Hansen, et al., "An Experimental and Kinetic Modeling Study on Dimethyl Carbonate (DMC) Pyrolysis and Combustion," Combust. Flame **164**, 224–238 (2016); DOI: 10.1016/j.combustflame.2015.11.019.
41. G. P. Smith, D. M. Golden, M. Frenklach, et al., "GRI-Mech 3.0," http://www.me.berkeley.edu/gri_mech/.
42. F. N. Egolfopoulos et al., "Advances and Challenges in Laminar Flame Experiments and Implications for Combustion Chemistry," Prog. Energy Combust. Sci. **43**, 36–67 (2014); DOI: 10.1016/j.pecs.2014.04.004.
43. P. D. Ronney and H. Y. Wachman, "Effect of Gravity on Laminar Premixed Gas Combustion. I: Flammability Limits and Burning Velocities, Combust. Flame **62** (2), 107–119 (1985); DOI: 10.1016/0010-2180(85)90139-7.
44. A. P. Kelley, G. Jomaas, and C. K. Law, "Critical Radius for Sustained Propagation of Spark-Ignited Spherical Flames," Combust. Flame **156** (5), 1006–1013 (2009); DOI: 10.1016/j.combustflame.2008.12.005.
45. M. I. Hassan, K. T. Aung, O. C. Kwon, and G. M. Faeth, "Properties of Laminar Premixed Hydrocarbon/Air Flames at Various Pressures," J. Propul. Power **14** (4), 479–488 (1998); DOI: 10.2514/2.5304.
46. V. Pokorný, V. Štejfa, M. Fulem, et al., "Vapor Pressures and Thermophysical Properties of Dimethyl Carbonate, Diethyl Carbonate, and Dipropyl Carbonate," J. Chem. Eng. Data **62** (10), 3206–3215 (2017); DOI: 10.1021/acs.jced.7b00295.